This article has been accepted for publication in a future issue of this journal, but has not been fully edited. Content may change prior to final publication. Citation information: DOI 10.1109/TMECH.2019.2892069, IEEE/ASME Transactions on Mechatronics

Uncertainty Based IMU Orientation Tracking Algorithm for Dynamic Motions

Qilong Yuan, *Member, IEEE,* Ehsan Asadi, *Member, IEEE,* Qinghua Lu, Guilin Yang, *Member, IEEE*, I-Ming Chen, *Fellow, IEEE, ASME*.

***Abstract*— With the recent technological advancement in low-cost wireless inertial motion trackers, measuring 3D motion for biomechanics research becomes more facile. However, the methods of acceleration modeling in off-the-shelf filters do not hold for all movements in sports activities with significant and long-lasting accelerations. This paper presents a robust algorithm for orientation tracking in the presence of large active accelerations lasting longer than the maximum time the MEMS gyroscopes can solely keep track of the body orientation. We particularly model the uncertainty of active acceleration and take it into explicit account in an Extended Kalman Filter (EKF) based orientation estimator for applying measurement updates accurately in dynamic motions like sports activities. The proposed tracker also estimates the magnetic disturbances by using an uncertainty model, to improve the heading estimation. Benchmarking the results with the Vicon Optical as ground truth and the MTw kit with a specific filter for body motion tracking shows the robustness of our method against variations of acceleration in different types of motion. Our tracker performs orientation estimation in real time with fast convergence during acceleration shocks and low Root Mean Square Error (RMSE), particularly when experiencing large accelerations in periodic motions.**

I. Introduction

Nowadays, many motion capture suits are developed using Inertial Measurement Units (IMU) [1-9], and they will become much smaller and cheaper with the advancement of MEMS technologies [10, 11]. Measuring 3D motion is challenging in biomechanics, kinematics, and sports as it requires sensors that allow for free body movement [12]. Thus, wireless inertial tracking technology is necessary in such applications. Considering these requirements, Xsens Technologies introduces the MTw [13], a wireless inertial motion tracker, specifically developed for 3D motions without the need of tracker-host cabling. These types of sensors now tend to become an alternative to expensive optical motion capture systems. But, applications like biomedical science and sports research require more robust and accurate orientation estimation in various dynamic motion conditions [5].

Typically, Kalman Filter or EKF is used in the sensor fusion algorithms, [1, 2, 14, 15], to estimate and track the 3D orientation of body, upon the combined integration of measurements provided by a 3-axis gyroscope, a 3-axis accelerometer, and 3- axis magnetometer. In the Kalman based orientation estimators, the gyro's angular rate is integrated to predict the orientation in a short period, but the estimation drifts gradually over time due to the measurement biases. Then, the errors are corrected using the magnetic strength and acceleration readings concerning the gravity reference and the local magnetic strength vector. The accelerometer model is used to express the effect of both gravity and other acceleration due to the body motion and the accuracy of model has a substantial impact on the measurement update of roll and pitch orientations. In tracking daily dynamic actions, the acceleration of larger than 5g is widespread that needs to be treated carefully. Similarly, the magnetometer model expresses the influence of both the earth's magnetic field and other magnetic objects on the heading angle. The magnetic disturbance is substantial in most indoor applications [16, 17]. However, many works in body motion tracking consider low acceleration or assume that long-term acceleration due to motion is zero and the magnetic disturbances are low. As a result, most of these methods show different performances in static and dynamic conditions[6, 14, 16, 18-21].

Daniel et al. model the acceleration as low-pass filtered white noise [16] but does not study the covariance calculation of the white noise. These algorithms work well for slow motions. However, the accuracy of this type of methods is sensitive to the speed of movements because the approximate acceleration model does not hold in fast actions [16]. In general, sensors are much less accurate during rapid motions than slow motions, and more robust methods are needed for motion tracking in the dynamic movements.

Reference [22] proposed a threshold method to capture the low active acceleration phase and to correct the inclination error only during this period. However, there are typical cases that the threshold will not be satisfied during the long duration due to the active acceleration, causing incremental drift in orientation estimates. Lee used the low-pass filtering model to estimate the acceleration in a Kalman filter. In reference [22] maximum acceleration of 37.22 m/s2 was tested during periodic motions. Such model encounters large errors in acceleration estimation during motions with irregular accelerations and does not calculate the covariance matrix of the acceleration correctly. In summary, imprecise acceleration model will cause large inclination errors and delay the convergence in inclination tracking.

Another way of orientation estimation in the conditions stated above is to rely mainly on the gyroscopes readings and

This project is partially supported by National Natural Science Foundation, China, (51705076 and 51475448). Corresponding Author: Qilong Yuan, School of Electro-Mechanical Engineering, Foshan University, 528000, China.

This article has been accepted for publication in a future issue of this journal, but has not been fully edited. Content may change prior to final publication. Citation information: DOI 10.1109/TMECH.2019.2892069, IEEE/ASME Transactions on Mechatronics

selectively detect when to apply measurement updates using the accelerometers or magnetometers [23, 24]. The solution is to implement hypothesis detectors on the measurements but requires prior knowledge about the system dynamic, where a zero velocity phases are needed. The idea to detect stationary phases of IMU and correct the orientation is interesting, but it is not practical for variation of continuous motions where stationary phases are not available. Such idea indicates that the majority of quick actions have motion phases with low active acceleration that is not the same as stationary.

Bachmann assumes that the integration of the acceleration over a fixed period to be zero [25]. Similarly, many off-the-shelf inertial motion trackers such as the MTw kit by Xsens, use filters with the assumption that the average acceleration during some time is zero [13]. During this time, the gyroscopes must be able to track the orientation accurately. We conducted a benchmark study of the MTw's accuracy in different types of dynamic motion tracking, using the VICON OPTICAL capture system as the ground truth. Benchmark results show that estimation accuracy is dependent on the types of active movement. Such methods are mainly best for slow-motion tracking [26], but for some applications, this assumption does not hold. For example, dynamic motions in the running, continuous jumping and leg swinging generate significant and varying accelerations far from an on-average zero acceleration Thus, the zero on-average acceleration model [13] could degrade the accuracy of the orientation estimates due to the mismatch between the actual application and the assumption. Matthew [14] also has similar comments on the issue of dynamic motion tracking. Measurement error is evident during motions with significant angular velocity and large and irregular acceleration. That study concludes that unreliable acceleration should be avoided in orientation correction to prevent large inclination errors.

We propose a new IMU-based algorithm for orientation tracking in the presence of large active accelerations after the peak-period of dynamic motions, such as jumping or running. Our method introduces an uncertainty-based fusion method to make the best use of accelerometer measurements in applying EKF-based measurement updates that can track the orientation of dynamic motions accurately. The proposed tracker also handles magnetic disturbances in estimating the heading by using a magnetic disturbance uncertainty model. Various experiments including running, leg swinging, and jumping with dynamic motions, acceleration and angular velocity larger than 6g and10rad/s, regularly, are used to verify the accuracy and robustness of the algorithm. Experimental results are benchmarked with an optical tracking system and compared with the MTw kit by Xsens with a specific filter for body motion tracking. The results indicate that our method is more robust in adapting to the variation of different types of motion and in overcoming sudden inclination errors during acceleration shocks (and magnetic disturbances). The estimates converge more quickly, and the drifting error in heading angle is also reduced. Such improvements can contribute to improving the efficiency of motion tracking devices in particular applications by using economical and convenient sensors. We make efficient use of the low acceleration phase for inclination correction and magnetometer readings for heading correction by incorporating a precise uncertainty model of active acceleration and magnetic disturbance

The remaining parts of the paper are arranged as follows. Section II introduces the measurement models of the sensors in IMU. Section III introduces the theory of the tracking method. Section IV elaborates on the experimental setup. Section V explains the experimental results. Section VI discusses the algorithm and analyses its efficiency in orientation tracking. Finally, the paper is concluded in Section VII.

II. IMU-Based Measurement Models

A. Static Orientation Estimation

When the IMU is in **stationary** position, the measurement of the accelerometer $\boldsymbol{a_f}$ in the sensor frame is represented by ${}^{S}\boldsymbol{a_g}$. In this work, it is assumed that the IMU is calibrated, so the scalar and constant bias are not shown in the model: ${}^{S}\boldsymbol{a_g}$ is the acceleration signal caused by gravity, with bias removed from the measurement. The measurement of the magnetic sensor $\boldsymbol{m_m}$ is a combination of the local magnetic strength represented in sensor frame ${}^{S}\boldsymbol{m_0}$ and noises (disturbances and white noises). When there is no magnetic disturbance and noise, we have $\boldsymbol{m_m = m_0}$.

Let $\boldsymbol{R_s}$ denotes the rotational matrix of the sensor frame. The IMU's reference frame is defined based on the gravity and the local magnetic field. This way, the z-axis is directed along the $\boldsymbol{a_f}$ direction (upward), and y is pointed along the $\boldsymbol{a_f \times m_m}$ direction (as shown in Fig. 1). Thus, we have

$$\begin{cases} {}^{S}_{G}\boldsymbol{z} = \dfrac{\boldsymbol{a_f}}{\|\boldsymbol{a_f}\|} \\ {}^{S}_{G}\boldsymbol{y} = \dfrac{\boldsymbol{a_f \times m_0}}{\|\boldsymbol{a_f \times m_0}\|} \\ {}^{S}_{G}\boldsymbol{x} = {}^{S}_{G}\boldsymbol{y} \times {}^{S}_{G}\boldsymbol{z} \end{cases} \tag{1}$$

$$\boldsymbol{R_{s,0}} = [{}^{S}_{G}\boldsymbol{x} \quad {}^{S}_{G}\boldsymbol{y} \quad {}^{S}_{G}\boldsymbol{z}]^{T} \tag{2}$$

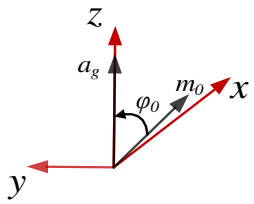

Fig. 1. The Defined Reference frame of IMU.

B. Integrating Angular Rates Over Time

The measurement of gyroscope is consisting of the active angular velocity $\boldsymbol{\omega_t}$, the bias $\boldsymbol{b_w}$ and the white noise $\boldsymbol{w_{g,t}}$. Thus, we have,

$$\boldsymbol{\omega_{g,m} = \omega_t + b_w + w_{g,t}}\ , \tag{3}$$

where $\boldsymbol{\omega_t}, \boldsymbol{b_w}, \boldsymbol{w_{g,t}} \in \Re^{3\times 1}$. The time-control process of the gyroscope bias is driven by a white noise $\boldsymbol{w_{b,t}}$. So, we have,

$$\boldsymbol{b_{w,t} = b_{w,t-1} + w_{b,t}}. \tag{4}$$

With correct calculation of the initial orientation, the orientation of the sensor can be updated based on integrating the angular velocity as follows,

This article has been accepted for publication in a future issue of this journal, but has not been fully edited. Content may change prior to final publication. Citation information: DOI 10.1109/TMECH.2019.2892069, IEEE/ASME Transactions on Mechatronics

$$\boldsymbol{R_{s,k}} = \boldsymbol{R_{s,k-1}} \cdot rotz\big(dt \cdot \omega_{g,k}(3)\big) \cdot roty\big(dt \cdot \omega_{g,k}(2)\big) \cdot rotx(dt \cdot \omega_{g,k}(1)) \quad (5)$$

where $roti(\theta)$ is a *SO(3)* matrix corresponding to a rotation around axis i, a given angle θ and the time interval dt. Such integrating updates will introduce errors to the orientation estimation due to the accumulation of angular velocity errors. Let $\delta\theta$ denotes the orientation error of the sensor, $\delta\theta \in \Re^{3\times1}$. Then, the actual orientation $\boldsymbol{R_s^+}$ can be corrected as follows,

$$\boldsymbol{R_s^+} = \boldsymbol{R_s} \cdot rotz(\delta\theta(3)) \cdot roty(\delta\theta(3)) \cdot rotx(\delta\theta(3)). \quad (6)$$

In such a way, the result is more accurate than the linear approximation $\boldsymbol{R_s^+} = \boldsymbol{R_s}\big(\boldsymbol{I} + \boldsymbol{\delta\hat{\theta}}\big)$ as introduced in [13, 16, 27], and no re-orthogonalization of the updated matrix $\boldsymbol{R_{s,k}}$ and $\boldsymbol{R_s^+}$ is needed since they belong to $\boldsymbol{SO}(3)$.

C. Measurements of Accelerometers and Magnetometer

In IMU-based orientation $\boldsymbol{R_s}$ tracking, the angular drifting error from the angular velocity integration $\boldsymbol{\omega_{g,m}}$ need to be corrected, through using the acceleration and the magnetometer measurements $\boldsymbol{a_f}$ and $\boldsymbol{m_m}$. We can prove that orientation error $\boldsymbol{\delta\theta}$ is observable from the measurements of accelerometer and the magnetometer if the active acceleration $\boldsymbol{a_t}$, and the magnetic disturbance $\boldsymbol{m_d}$ are properly estimated (see Fig. 2), as long as the local magnetic strength vector $\boldsymbol{m_0}$ and gravitational accelerometer are not collinear with each other [17].

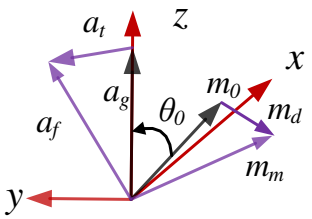

Fig 2. Illustration of the accelerometer and the magnetometer measurements.

1) Acceleration Measurement Model

The accelerometer measurements consist of the acceleration caused by gravity and the active acceleration, as shown in Fig 2. Let $\boldsymbol{a_f}$, $\boldsymbol{a_t}$, and $\boldsymbol{w_a}$ denote the accelerometer measurement, the active acceleration and the acceleration white noise, respectively, (all in sensor frame). Then, we have,

$$\boldsymbol{a_f} = \boldsymbol{R_s^{+T}}\boldsymbol{g} + \boldsymbol{a_t} + \boldsymbol{w_a}\,, \quad (7)$$

where $\boldsymbol{g} = \mathrm{g}\boldsymbol{z}; \boldsymbol{z} = [0 \quad 0 \quad 1]^{\mathrm{T}}$, and g is local gravitational acceleration (absolute value). Based on Equation (6), we have,

$$\boldsymbol{a_f} = [\boldsymbol{R_s}\big(\boldsymbol{I} + \boldsymbol{\delta\hat{\theta}}\big)]^{\boldsymbol{T}}\boldsymbol{g} + \boldsymbol{a_t} + \boldsymbol{w_a}\,. \quad (8)$$

Thus,

$$\boldsymbol{a_f} = g\boldsymbol{R_s}^{\boldsymbol{T}}\boldsymbol{z} + g\boldsymbol{R_s}^{\boldsymbol{T}}\boldsymbol{z} \times \boldsymbol{\delta\theta} + \boldsymbol{a_t} + \boldsymbol{w_a}\,. \quad (9)$$

Noticing that $\boldsymbol{a_f}$ can be very significant in dynamic motions, and to ensure the error is bounded, the accelerometer measurement is normalized as follows,

$${}^{s}\boldsymbol{n_a} = \frac{\boldsymbol{a_f}}{\|\boldsymbol{a_f}\|} = \frac{\boldsymbol{1}}{\|\boldsymbol{a_f}\|}\big(g\boldsymbol{R_s}^{\boldsymbol{T}}\boldsymbol{z} + g\boldsymbol{R_s}^{\boldsymbol{T}}\boldsymbol{z} \times \boldsymbol{\delta\theta} + \boldsymbol{a_t} + \boldsymbol{w_a}\big). \quad (10)$$

Finally, considering $\boldsymbol{w_n} = \boldsymbol{a_t} + \boldsymbol{w_a}$, Equation (10) is simplified as

$${}^{s}\boldsymbol{n_a} = \frac{\boldsymbol{1}}{\|\boldsymbol{a_f}\|}(g\boldsymbol{R_s}^{\boldsymbol{T}}\boldsymbol{z} + g\boldsymbol{R_s}^{\boldsymbol{T}}\boldsymbol{z} \times \boldsymbol{\delta\theta} + \boldsymbol{w_n})\,. \quad (11)$$

2) Magnetometer Measurement

The magnetometer measurement is consisting of the local earth magnetic and the disturbances, as shown in Fig 2. Let $\boldsymbol{m_m}$, $\boldsymbol{m_0}$, $\boldsymbol{m_d}$ and $\boldsymbol{w_m}$ denote the magnetometer measurement, the local reference magnetic strength, the magnetic disturbance, and the white noise in magnetometer measurement, respectively. Then

$$\boldsymbol{m_m} = \boldsymbol{R_s^{+T}}\boldsymbol{m_0} + \boldsymbol{m_d} + \boldsymbol{w_m}\,. \quad (12)$$

Based on Equation (6), we have,

$$\boldsymbol{m_m} = [\boldsymbol{R_s}\big(\boldsymbol{I} + \boldsymbol{\delta\hat{\theta}}\big)]^{\boldsymbol{T}}\boldsymbol{m_0} + \boldsymbol{m_d} + \boldsymbol{w_m}\,. \quad (13)$$

Therefore, we have,

$$\boldsymbol{m_m} = \boldsymbol{R_s}^{\boldsymbol{T}}\boldsymbol{m_0} + \boldsymbol{R_s}^{\boldsymbol{T}}\boldsymbol{m_0} \times \boldsymbol{\delta\theta} + \boldsymbol{m_d} + \boldsymbol{w_m}\,. \quad (14)$$

III. Uncertainty Based Fusion of IMU's Readings for Dynamic Motion Tracking

In this work, we particularly model the uncertainty of active acceleration and take it into explicit account in an EKF based orientation estimator for applying measurement updates accurately in dynamic motions.

Considering the measurement model of acceleration, Eqs. (7)-(11), we propose to approximate the active acceleration, a_t, *as white noise* as follow,

$$\boldsymbol{a_{t,x\,(y,z)}} \backsim \boldsymbol{N}(\boldsymbol{0}, S_{at}\,),$$

where S_{at} is the **uncertainty of active acceleration** and it is accurately modeled in the following section III.1, without a pre-knowledge of a_t. The active acceleration and the noise are considered as white noise with $\boldsymbol{R_{at}}$ being the covariance matrix. Thus,

$$\boldsymbol{R_{at}} = {S_{at}}^2\boldsymbol{I_{3\times3}} + \boldsymbol{R_a}\,. \quad (15)$$

In addition, the uncertainty $\boldsymbol{Q_{md}}$ of magnetic disturbances $\boldsymbol{m_d}$ is estimated as well, Sec. III.2, and it is incorporated in time update of EKF.

Accordingly, the working flow of the proposed method for fusing IMU-based measurements is shown in Fig 3.

The States of the EKF is chosen to be the orientation errors, $\boldsymbol{\delta\theta}$, the gyro offset, $\boldsymbol{b_w}$, and the magnetic disturbances, $\boldsymbol{m_d}$, as follows.

$$\boldsymbol{x} = [\boldsymbol{\delta\theta}^{\boldsymbol{T}}, \boldsymbol{b_w}^{\boldsymbol{T}}, \boldsymbol{m_d}^{\boldsymbol{T}}]^{\boldsymbol{T}} \quad (16)$$

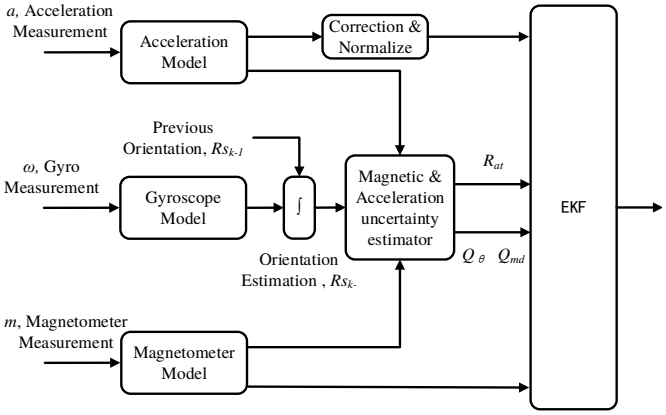

Fig 3. Workflow of the Proposed Uncertainty Based Fusion of IMU's Readings

This article has been accepted for publication in a future issue of this journal, but has not been fully edited. Content may change prior to final publication. Citation information: DOI 10.1109/TMECH.2019.2892069, IEEE/ASME Transactions on Mechatronics

A. *Uncertainty Models*

Inclination correction during the low acceleration period and heading correction in the presence of a small magnetic disturbance are efficient. But estimating the value of active acceleration, Fig.4, during the variation of dynamic activities is very challenging. Therefore, how to capture orientation in such period by making the best use of all measurements become a critical problem in IMU-based dynamic motion tracking. This issue could be addressed by accurate modeling of the uncertainty of the active acceleration, instead of direct estimation of active acceleration.

1) *Uncertainty of active acceleration*

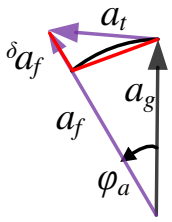

Fig 4. Illustration of active acceleration estimation

At any particular time *t*, with accelerometer measurement $\boldsymbol{a_f}$, and *without other pre-knowledge of the active acceleration* $\boldsymbol{a_t}$, the magnitude of $\boldsymbol{a_t}$ can be expressed based on Equation (7). As illustrated in Fig 4. **,** where φ_a denotes the angle between a_g (upward) and a_f (zero when $\boldsymbol{a_t} = \boldsymbol{0}$), and δa_f denotes the magnitude difference between $\boldsymbol{a_f}$ and g,

$$\begin{cases} \delta\varphi_a = \arccos\left(\frac{{}^{s}\boldsymbol{z_e}\cdot\boldsymbol{a_f}}{\|\boldsymbol{a_f}\|}\right) \\ \left|\|\boldsymbol{a_f}\| - \mathrm{g}\right| = \delta a_f \end{cases}, \tag{17}$$

where ${}^{s}\boldsymbol{z_e} = \boldsymbol{R_s}^{T}[\boldsymbol{0},\boldsymbol{0},\boldsymbol{1}]^{T}$.

It is clear that when φ_a and δa_f are small, we have,

$$\|\boldsymbol{a_t}\|^2 \approx \delta {a_f}^2 + (\delta\varphi_a \mathrm{g})^{\boldsymbol{2}}, \tag{18}$$

where $\delta {a_f}^2$ is caused by the magnitude difference and $(\delta\varphi_a \mathrm{g})^{\boldsymbol{2}}$ is caused by the angular difference. Here, the uncertainty of the active acceleration is defined by the following function,

$${S_{at}}^2 = \mu_s(\delta {a_f}^2 + (\delta\varphi_a \mathrm{g})^{\boldsymbol{2}}), \tag{19}$$

where μ_s is the coefficient to be adjusted in filter tuning.

In such estimation of $\delta\varphi_a$, the estimated Z-axis of the sensor frame ${}^{s}\boldsymbol{z_e}$ is applied. Therefore, the closer the $\boldsymbol{a_f}$ is to $\boldsymbol{a_g}$, the faster the inclination result converges.

It is clear that when the active acceleration $\boldsymbol{a_t}$ is very small ($\boldsymbol{a_t} + \boldsymbol{w_z} \approx \boldsymbol{0}$, and $\|\boldsymbol{a_f}\| \approx g$), the uncertainty S_{at} is also small, and the above equation yields to

$${}^{s}\boldsymbol{n_a} = \frac{\boldsymbol{a_f}}{\|\boldsymbol{a_f}\|} \approx \boldsymbol{R_s}^{T}\boldsymbol{z} + \boldsymbol{R_s}^{T}\boldsymbol{z} \times \boldsymbol{\delta\theta} = {}^{s}\boldsymbol{z_p} + {}^{s}\boldsymbol{z_p} \times \boldsymbol{\delta\theta}. \tag{20}$$

When $\boldsymbol{a_t}$ is significant, such model in Equation (19) lead to a large uncertainty and thus not reliable. By considering this uncertainty model in measurement update of Kalman filtering. All the large accelerations contribute little in inclination correction, while the low accelerations are still incorporated efficiently in measurement update.

In Xsens, the estimated active acceleration $\boldsymbol{a_t}$ is modeled as low-pass filtered noise, and the $\boldsymbol{a_g}$ is estimated through removing estimated $\boldsymbol{a_t}$ from measurement $\boldsymbol{a_f}$. When the active acceleration is very large and dynamic, the errors of acceleration estimation is substantial and thus lead to inaccurate estimation of the inclination and the noise covariance. This is because, **g** is used to estimate the value of $|\boldsymbol{a_f} - \boldsymbol{a_{t,w}}|$, where $\boldsymbol{a_{t,w}}$ is not an accurate estimation of $\boldsymbol{a_t}$.

Please take note that, when $\|\boldsymbol{a_f}\|$ is near to zero, it means, the object is experiencing a motion near to free falling, e.g. when you through the IMU in space. In such condition, there is no reliable reference for inclination correction, and therefore, the measurement from acceleration estimation is not used for orientation correction when the magnitude is small (2 m/s^2 for example).

2) *Uncertainty of Magnetic Disturbance*

Similar to active acceleration, the uncertainty of magnetic disturbance $\boldsymbol{m_d}$ is estimated by the following Equation (20) and (21).

$$\begin{cases} \delta\varphi_m = \operatorname{acos}\left(\frac{{}^{s}\boldsymbol{m_{0e}}\cdot\boldsymbol{m_m}}{\|{}^{s}\boldsymbol{m_{0e}}\|\cdot\|\boldsymbol{m_m}\|}\right) \\ \left|\|\boldsymbol{m_m}\| - \|\boldsymbol{m_0}\|\right| = \delta m_m \end{cases} \tag{21}$$

$${S_m}^2 = \mu_m(\delta {m_m}^2 + (\delta\varphi_m\|\boldsymbol{m_m}\|)^2) \tag{22}$$

where μ_m is the coefficient to be adjusted in filter tuning.

Referring to [16], the magnetic disturbance is modeled as the following time-control process,

$$\boldsymbol{m_{d,k}} = c_d\boldsymbol{m_{d,k-1}} + \boldsymbol{w_d}\,, \tag{23}$$

where, c_d is a constant between 0 to 1, and $\boldsymbol{w_d}$ is the white noise driven by ${S_m}^2$. Thus, the process noise covariance matrix is as follows,

$$\boldsymbol{Q_{md}} = {S_m}^2\boldsymbol{I_{3\times3}}\,. \tag{24}$$

B. *EKF-Based Data Fusion*

The Extended Kalman filter is used to addresses the problem of estimating the state $\boldsymbol{x}$ of a discrete-time controlled process that is governed by a non-linear stochastic difference equation,

$$\boldsymbol{x_k} = f(\boldsymbol{x_{k-1}}, \boldsymbol{u_{k-1}}, \boldsymbol{w_{k-1}})\,, \tag{25}$$

with a measurement $\boldsymbol{z}$

$$\boldsymbol{z_k} = \boldsymbol{h}(\boldsymbol{x_k}, \boldsymbol{v_k})\,. \tag{26}$$

The main formulation of EKF is given in Appendix I.

In this work, the normalized acceleration and the magnetic signal are used as the input measurements. We propose explicit incorporation of the estimated acceleration uncertainty, using Eq. 19, and the uncertainty of magnetic disturbance, using Eq. 24 in the EKF for measurement and time updates, correspondingly.

1) Time update process

Based on Equation (3), (4), the time-control process of the angular error $\boldsymbol{\delta\theta}$ is given as,

$$\boldsymbol{\delta\theta_k} = \boldsymbol{\delta\theta_{k-1}} + \boldsymbol{dt}(\boldsymbol{b_{w,k-1}} + \boldsymbol{w_{g,t}} + \boldsymbol{w_{b,t}})\,. \tag{27}$$

Consider the EKF state update function is as follows,

$$\boldsymbol{x_k} = \boldsymbol{A}\boldsymbol{x_{k-1}} + \boldsymbol{w_{k-1}}\,, \tag{28}$$

where $\boldsymbol{A} = \begin{bmatrix} \boldsymbol{I_{3\times3}} & \boldsymbol{dtI_{3\times3}} & \boldsymbol{0_{3\times3}} \\ \boldsymbol{0_{3\times3}} & \boldsymbol{I_{3\times3}} & \boldsymbol{0_{3\times3}} \\ \boldsymbol{0_{3\times3}} & \boldsymbol{0_{3\times3}} & c_d\boldsymbol{I_{3\times3}} \end{bmatrix}, \boldsymbol{w_{k-1}} = \begin{bmatrix} (\boldsymbol{w_{g,t}} + \boldsymbol{w_{b,t}})\boldsymbol{dt} \\ \boldsymbol{w_{b,t}dt} \\ \boldsymbol{w_d} \end{bmatrix}$

The initial estimation of the $\boldsymbol{\delta\theta}$ and $\boldsymbol{b_w}$ at each discrete time are set to be zeros before filtering. Then, we have

This article has been accepted for publication in a future issue of this journal, but has not been fully edited. Content may change prior to final publication. Citation information: DOI 10.1109/TMECH.2019.2892069, IEEE/ASME Transactions on Mechatronics

$$\boldsymbol{x}_{-} = [\boldsymbol{0}_{6\times1}; \boldsymbol{m}_{d0}]. \quad (29)$$

The covariance matrix of the state time-control process noise $\boldsymbol{w}_{k-1}$ are:

$$\boldsymbol{Q} = \begin{bmatrix} \boldsymbol{dt}^2(\boldsymbol{Q}_\omega + \boldsymbol{Q}_b) & \boldsymbol{dtQ}_b & \boldsymbol{0}_{3\times3} \\ \boldsymbol{dtQ}_b & \boldsymbol{Q}_{wb} & \boldsymbol{0}_{3\times3} \\ \boldsymbol{0}_{3\times3} & \boldsymbol{0}_{3\times3} & \boldsymbol{Q}_{md} \end{bmatrix} \quad (30)$$

As shown in [16], the filter of XSENS set A to be zero, and the covariance matrix between $\boldsymbol{\delta\theta}$ and $\boldsymbol{b}_w$ is set to be $\boldsymbol{dt}^2\boldsymbol{Q}_b$, which in our model is modified to be $\boldsymbol{dtQ}_b$ based on the proposed process model Eq. 27.

2) Measurements Model and Update

The measurement model is as follows,

$$\boldsymbol{z}_{m,k} = \boldsymbol{h}(\boldsymbol{x}_k, \boldsymbol{w}_{M,k}) = \boldsymbol{H}_k\boldsymbol{x}_k + \begin{bmatrix} \frac{\boldsymbol{R}_S^T\boldsymbol{g}}{\|\boldsymbol{a}_f\|} \\ \boldsymbol{R}_S^T\boldsymbol{m}_0 \end{bmatrix} + \boldsymbol{v}_{M,k}, \quad (31)$$

where $\boldsymbol{v}_{M,k} = \begin{bmatrix} \boldsymbol{w}_n \\ \boldsymbol{w}_m \end{bmatrix}$.

Based on Equation (12) and (18), we have

$$\boldsymbol{H}_k = \begin{bmatrix} \frac{(\boldsymbol{R}_S^T\boldsymbol{g})^\wedge}{\|\boldsymbol{a}_f\|} & \boldsymbol{0}_{3\times3} & \boldsymbol{0}_{3\times3} \\ (\boldsymbol{R}_s{}^T\boldsymbol{m}_0)^\wedge & \boldsymbol{0}_{3\times3} & \boldsymbol{I}_{3\times3} \end{bmatrix}, \quad \boldsymbol{V}_k = \boldsymbol{I}_{6\times6} \quad (32)$$

The covariance of $\boldsymbol{w}_z$ and $\boldsymbol{w}_m$ are estimated based on white noise model.

$$\boldsymbol{R}_k = \begin{bmatrix} \boldsymbol{R}_n & \boldsymbol{0}_{3\times3} \\ \boldsymbol{0}_{3\times3} & \boldsymbol{R}_m \end{bmatrix} = \begin{bmatrix} \frac{1}{\|\boldsymbol{a}_f\|^2}\boldsymbol{R}_{at} & \boldsymbol{0}_{3\times3} \\ \boldsymbol{0}_{3\times3} & \boldsymbol{R}_m \end{bmatrix} \quad (33)$$

With Equation (26) to (30), the EKF can be applied to update the states. The actual orientation $\boldsymbol{R}_s^+$ can be updated by Equation (6).

3) *Covariance Setting*

The value of $\boldsymbol{Q}_\omega + \boldsymbol{Q}_b$ defines the stiffness of the time integration process in the EKF. Thus, when the gyroscope is very well calibrated, $\boldsymbol{Q}_\omega$ and $\boldsymbol{Q}_b$ are very small and the tracking will benefit from the accurate integration process. When the estimated gravity is accurate, $\boldsymbol{R}_n$ is small that ensure efficient inclination correction. Similarly, $\boldsymbol{R}_m$ is small when the magnetic measurement is close to the local magnetic reference. In our method, we update the value of $\boldsymbol{R}_n$ and $\boldsymbol{Q}_{md}$ during the motion by incorporating the proposed uncertainty models for active acceleration and magnetic disturbances.

IV. Experimental Setup

The raw measurements of MTw IMU sensor [29] is used in this work for evaluating our method. This sensor is specially designed for human motion tracking and provides both raw IMU data and the orientation estimates. The typical range of the angular velocity measurement is ±1200 deg/s (20.94rad/s). The typical range of the accelerometer is ±160m/s^2. Such wide ranges enable measuring the raw data in highly dynamic actions. More detailed specification of the sensor can be found in the Xsens technical manuals [29].

Multiple IMU sensors are mounted on the lower limbs (the pelvis, the right thigh, the right shank and the right foot separately.) to capture the lower limb motions as shown in Fig. 6. Data sampling rate is 50Hz for IMU .

Fig. 5. Attachment of Markers on IMU Sensor

Fig. 6. Experiment Setups: IMU and Optical System

To conduct a benchmark experiment, a VICON motion capture system with eight optical cameras is used as a reference. The coverage area of the system in the lab is 6m by 5m. Three reflective optical markers are rigidly attached to each Xsens sensor as shown in Fig. 6. Therefore, while the Xsens IMU moves, the both systems capture the motion simultaneously. As the three markers can fully define the orientation of the IMU, the estimates of the two systems can be compared after synchronization and by presenting them in the same reference coordinate frame. The accuracy of positioning marker by a calibrated Vicon is reported to be 0.1mm, resulting in an angular accuracy at the magnitude of 0.1 degrees in the testing setup. Data sampling rate is 100Hz for the VICON system in this experiment.

A. Benchmark Experiments

The purpose of benchmark experiment is to compare the orientation estimates by our tracking method, Xsens estimator and VICON system for different types of body motions regarding the variation in active body acceleration, angular velocity, and moving frequency. Therefore, we conducted the following experiment trials using realistic human movements:

a. Running experiment: the subject starts from standstill posture at the initial position, run forward to the end, turn back and then run again. (The maximum foot speed is 5.5m/s.)
b. Jump experiment: the subject starts from standstill posture at the initial position and jump continuously for three steps. Then, stop. (The total jumping length is about 3 meters.)
c. Swinging leg experiment: the subject starts from standstill posture at the initial position, then stand on the left foot and swing the right leg for 6-7 times. (The swing

This article has been accepted for publication in a future issue of this journal, but has not been fully edited. Content may change prior to final publication. Citation information: DOI 10.1109/TMECH.2019.2892069, IEEE/ASME Transactions on Mechatronics

frequency is about 1.5Hz, and the maximum foot velocity is 6m/s). Each motion repeated for four trails. The benchmarking method is introduced in [6].

V. Experimental Results

In this work, the Xsens outputs (shown in red color) and the outputs from our method (shown in black) are transformed into the same coordinate system and compared with the Vicon data (shown in blue color). To separate the inclination and heading errors, the Yaw Pitch and Roll Euler angles are used for presenting the comparison results.

The authors are aware of the technical details of commercial sensors and the proper function of the tested sensor in scenarios that exactly match the assumptions made by that specific sensor. However, based on theoretical and experimental analysis, the acceleration modeling of the deployed sensor does have drawbacks in some other applications, such as those which are studied in this work, with irregular movements and long-lasting large accelerations as the acceleration and its uncertainty are not well incorporated for tracking these scenarios.

For example, while jumping, the foot motion is highly dynamic with maximum acceleration >10g and angular velocity >17rad/s, which is calculated based on optical reference data. Under such conditions, the Xsens MTw produces large errors in the pitch estimation, as shown by the red line in Fig. 7. Besides, the error does not converge in time when the foot stops.

The proposed method manages to prevent the orientation error due to large acceleration and thus the results are much more accurate as shown by the black line which matches well with the reference (blue line).

In IMU-based orientation estimation, heading drift relies more on the magnetic measurement, and gravity estimation is only contributing in inclination error correction. It is more useful to know separately about the heading (yaw) drift and the inclination errors to see the efficiency of the algorithms. Thus, the two systems are compared through yaw, pitch, and roll angle orientations, which can be achieved via decomposition of the *SO(3)* rotational matrix in the form of ZYX Euler angle. Or [Yaw, Pitch, Roll] = $\text{Euler}_{ZYX}(R)$. Pitch angle is along the body sideward direction based on attachment, which is the main angular motion during gaits. The roll and yaw angle are compared in Fig. 8.

Table 1 provides the results of 4 jumping trails. It is clear that the new method reduces the angular errors during jumping motions. The errors in different trails vary, but in all the trails, the proposed method is able to avoid significant angular errors, unlike Xsens output, and the estimation converges very quickly when motion slows done.

Also, in the running test, the proposed method is more robust. As shown in Fig. 9, and Table 2, especially in pitch estimation. Our method can prevent large "overshooting" errors during such steps with high angular velocity and acceleration shocks, as shown by the red line in Fig. 9. Table 2 provides the results of 4 running trails. The roll and yaw angle are compared in Fig. 10.

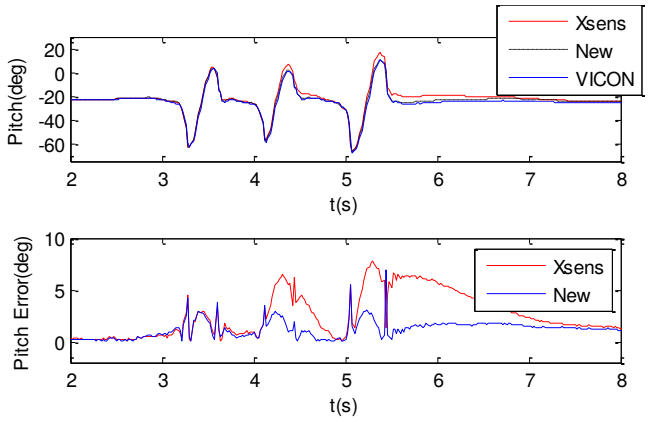

Fig. 7. Foot IMU: Pitch angle estimation while Jumping — Comparison between Xsens and proposed method

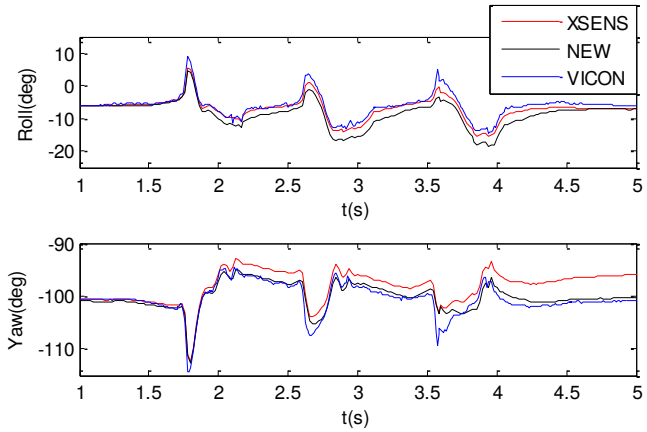

Fig. 8: Foot IMU: Roll and Yaw estimation while Jumping — Comparison between Xsens and proposed method.

Table 1 Comparison of jumping results of two methods

Foot Jumps	RMS Pitch (deg)	MAX Pitch (deg)	Yaw Error (deg)	RMS Angle (deg)	Max Angle (deg)	Max Accel	Max OMG (rad/s)
Xsens: 1	5.13	13.50	4.12	5.63	13.8	>10g	17
New:1	1.96	6.99	1.99	2.72	8.01		
Xsens: 2	1.58	8.10	4.13	3.35	8.54	>10g	17
New:2	1.05	6.88	1.93	2.52	7.60		
Xsens: 3	1.80	4.90	3.68	3.15	5.57	>10g	15
New:3	1.13	4.31	2.59	2.73	6.33		
Xsens: 4	4.27	13.97	6.10	6.00	14.01	>10g	15
New:4	1.58	6.69	2.31	3.00	8.22		

"**RMS Pitch**" and "**MAX Pitch**" denotes the root mean square error (RMSE) and the maximum error of pitch angle, respectively. "**Yaw Errors**" denotes the yaw error at the end of the motion. "**RMS Angle**" and "**Max Angle**" denotes the RMSE and the maximum errors in all directions, respectively. "**Max Accel**" and "**Max OMG**" denotes the maximum acceleration and angular velocity during the motion.

This article has been accepted for publication in a future issue of this journal, but has not been fully edited. Content may change prior to final publication. Citation information: DOI 10.1109/TMECH.2019.2892069, IEEE/ASME Transactions on Mechatronics

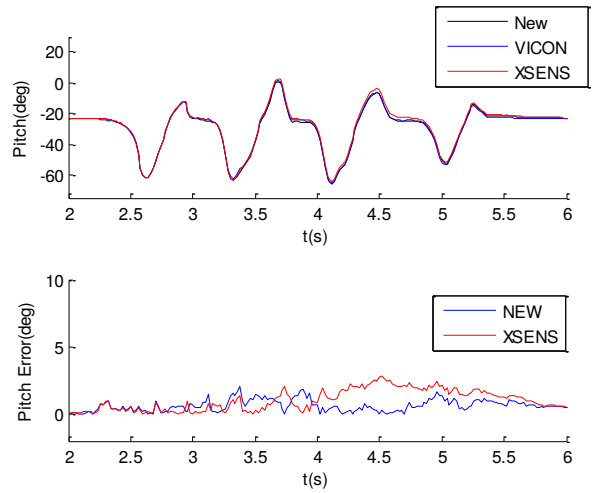

Fig. 9. Foot IMU Pitch Angle While Running—Comparison between XSESN and proposed method

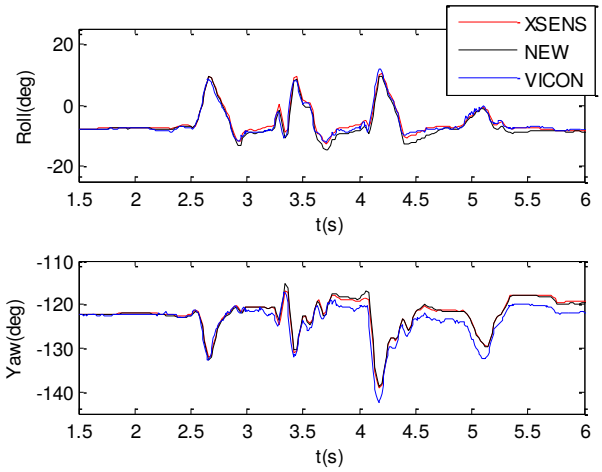

Fig. 10. Foot IMU Roll and Yaw While Running−Comparison between Xsens and proposed method.

Table 2 Comparison of running results of two methods

Foot Runs	RMS Pitch (deg)	MAX Pitch (deg)	Yaw Error (deg)	RMS Angle (deg)	Max Angle (deg)	Max Acc	Max OMG (rad/s)
Xsens :1	1.81	6.44	2.80	2.70	6.88	6g	9
New: 1	1.47	6.66	2.55	2.44	6.72		
Xsens :2	1.42	5.50	2.83	2.31	5.88	5g	8
New: 2	1.28	5.74	3.64	2.67	5.91		
Xsens :3	1.58	4.13	2.30	2.00	4.68	5g	9
New: 3	0.68	3.69	2.16	2.46	8.94		
Xsens :4	1.64	5.21	2.57	2.36	5.96	5g	8
New: 4	1.26	5.11	2.25	2.10	5.71		

Another extreme dynamic condition is continuous leg swinging motion. Such motion has high acceleration and high angular velocity. However, the moving frequency is relatively low. It is noticed that both the two methods show good convergence as shown in Fig. 11. Generally speaking, the maximum angular error by Xsens is consistent, and the error magnitude is also small, in this experiment.

The acceleration from the Xsens filtering algorithm [16] using a low-pass-filter to model the active acceleration is updated as follows,

$$\boldsymbol{a_t} = c_a \boldsymbol{a_{t-1}} + \boldsymbol{w_{at,t}} \tag{34}$$

where c_a defines the cut off frequency and $\boldsymbol{w_{at,t}}$ is said to be the white noise. In their model, the author mentioned that the covariance of $\boldsymbol{w_{at,t}}$ is $\boldsymbol{Q_{wa}}$, which seems to be constant in the filter.

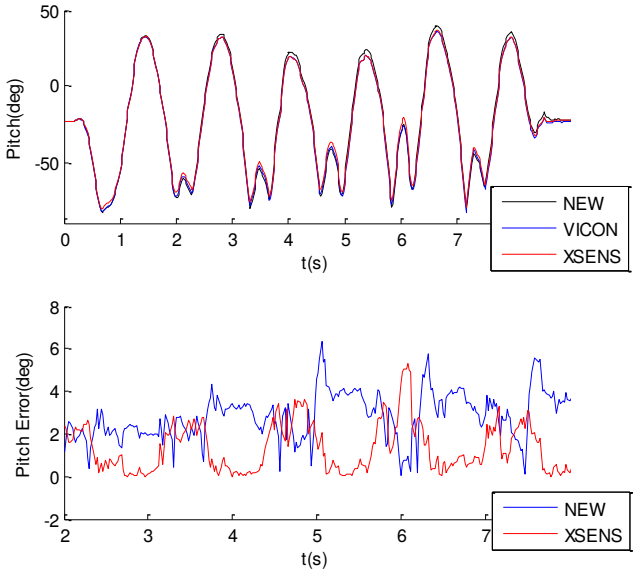

Fig. 11. Foot IMU Pitch Angle While Swinging—Comparison between Xsens and proposed method

Table 3 Comparison of Swinging Result of two methods

Foot Swings	RMS Pitch (deg)	MAX Pitch (deg)	Yaw Error (deg)	RMS Angle (deg)	Max Angle (deg)	Max Acc	Max OMG (rad/s)
Xsens:1	1.47	4.14	-2.15	2.12	4.38	6g	10
New:1	1.74	4.87	-3.09	3.56	8.34		
Xsens:2	2.04	5.50	-3.76	3.48	7.15	6g	10
New:2	2.20	5.07	-0.0445	3.21	7.48		
Xsens:3	1.10	2.49	-3.73	2.61	4.38	8g	10
New:3	2.01	7.65	-0.85	4.07	9.00		
Xsens:4	1.65	4.04	-5.15	3.42	5.52	8g	12
New:4	1.35	4.36	-2.12	4.39	9.97		

This article has been accepted for publication in a future issue of this journal, but has not been fully edited. Content may change prior to final publication. Citation information: DOI 10.1109/TMECH.2019.2892069, IEEE/ASME Transactions on Mechatronics

The applied model in Xsens, $\boldsymbol{w_{at,t} = a_t - c_a a_{t-1}}$, is inefficient when sudden acceleration shocks show up during jumping and running gaits and therefore results in large inclination errors as proved before. To improve this model, an automatically adjustable cutoff frequency is required according to the types of motions. Also, the covariance matrix of the process noise $\boldsymbol{w_{at,t}}$ need to be properly estimated.

The proposed method in this paper models the acceleration using white noise: $\boldsymbol{a_t = w_{at,t}}$, with well-estimated uncertainty. Thus, It is robust for all types of motions.

In the low-frequency motions, the low-pass filtering model in the active acceleration estimation can benefit our proposed method. We have tested that by applying $\boldsymbol{a_{fn} = a_f - c_a a_{t-1}}$ and use $\boldsymbol{{}^s n_a = \frac{a_{fn}}{\|a_{fn}\|}}$ in the filter. Using the proposed uncertainty estimation method, the performance of the filter improves during swinging motions as shown in Fig 12 (note that $\|\boldsymbol{a_{fn}}\|$can be very different from $\mathbf{g}$. Therefore, we don't use $\mathbf{g}$ to estimate $\|\boldsymbol{a_{fn}}\|$ in this algorithm, which is different from the method in [16, 30]).

The experiments also validate the efficiency of the introduced method in orientation tracking in variety of motions as tested on the human limbs.

VI. Discussion

In general, our method shows following improvements in dynamic motion tracking compared with existing algorithms:

1. The orientation estimator converges quickly after the peak-period of dynamic motions and acceleration shocks. Thus, no sudden and significant inclination error is experienced.
2. The process is robust in tracking short-term dynamic motions with high active acceleration that lasts longer than the maximum time the gyroscopes can solely keep track of the body orientation and it leads to low angular Root Mean Square Error.
3. The yaw drifting is also corrected with bounded heading errors.

The measured acceleration and angular velocity of different types of motions, namely walking, running, jumping and swinging have been shown in the Fig. 13 to illustrate the range of the acceleration and the angular velocity used in this work: the result is stacked horizontally from different experiments for clear comparison purposes. It can be noticed that the tested motions especially running, jumping and swinging have significant acceleration and angular velocities. Such motions are much more dynamic compared with the earlier works in IMU tracking [1-3,14-19,22-26].

In the experiments, the IMU is well calibrated and have reliable raw data. The accuracy of the gyroscope measurement is especially critical to provide a good accuracy in short periods. The measurement range of IMU should be sufficient (i.e. 1200deg/s and 16m/s^2 measurement range in angular rate and acceleration for MTw by Xsens) that can cover the full range of motion in the experiments.

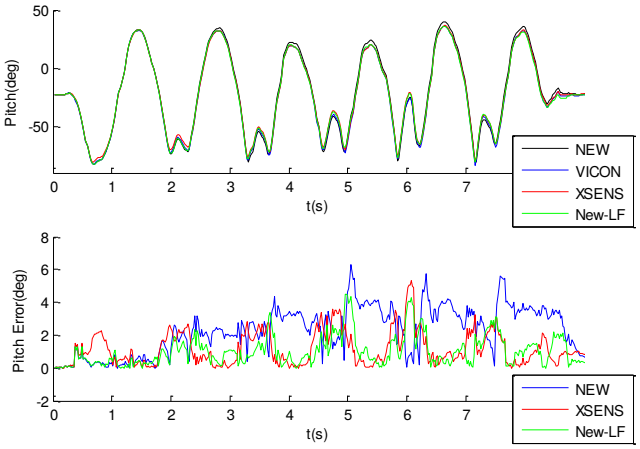

Fig. 12. Foot IMU Pitch Angle While Swinging outputs from XSESN, the proposed method and the modified method (New-LF) with low-frequency Acceleration Modeling

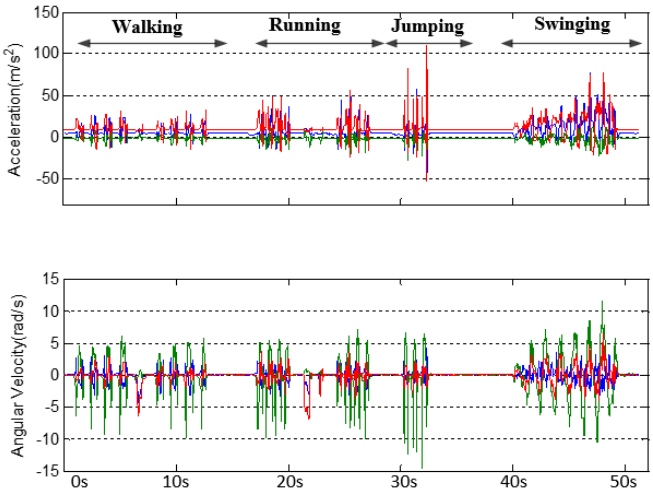

Fig. 13. Acceleration and Angular Velocity during different motions

A. *Analysis of the effects of acceleration uncertainty on the EKF-based orientation tracking*

1) *EKF-based Tracking and Acceleration Uncertainty*

EKF is an optimal tool to combine the information from gyro and accelerometer for inclination correction, In EKF, the uncertainty of the prediction is defined by $\boldsymbol{P_{k-1,\delta\theta}}$ (Please refer to Equation (27) to (30)). The influence of a new acceleration measurement on the estimate depends on the uncertainties of both the acceleration measurement and the state prediction by gyros, which are represented by $\boldsymbol{R_{at}}$ and $\boldsymbol{P_{k-1,\delta\theta}}$. As shown in Fig. 14, the center of the circles denotes the value of the estimated state from each estimation as indicated in the figure.

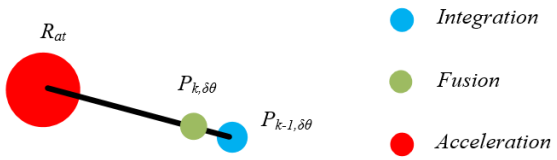

Fig. 14. Illustration of EKF in inclination correction

This article has been accepted for publication in a future issue of this journal, but has not been fully edited. Content may change prior to final publication. Citation information: DOI 10.1109/TMECH.2019.2892069, IEEE/ASME Transactions on Mechatronics

Given $\boldsymbol{P_{k-1,\delta\theta}}$, *and* $\boldsymbol{R_{at}}$, it is clear that the final estimation will be at a weighted value between the filtered result in the previous time interval and the current acceleration measurement. If the error of the acceleration measurement is significant, but the uncertainty is not considered to be correspondingly large, such error will be directly projected to the fused result, leading to large error of the sensor output.

2) *Slow inclination convergence by MTw Estimator*

According to the results of the jumping and running experiments, the estimation convergence of MTw by Xsens is slow in dynamic movement (as shown in Fig. 8 and Fig. 10). From the formulations and the sensor manual, it is known that this is because of the simple assumption of on-average zero acceleration and improper incorporation of accelerometer measurement and measurement's uncertainty during the dynamic phases. Actually, in a stationary phase, the measured acceleration is an almost exact reference of gravity, which can be seen from Equation (7) and (19)).

Due to the MTw configuration and its settings for process covariance during integration, $\boldsymbol{P_{k-1,\delta\theta}}$ is very small. Also, it is noticed that $\boldsymbol{R_a}$ is always set to be constant in MTw with a value much larger than $\boldsymbol{P_{k-1,\delta\theta}}$. Thus, the data fusion is mainly dependent on the integration of gyro measurement, and the correction from acceleration measurement will be very slow. Therefore, once a large error is caused, the estimation convergence is very slow. This phenomenon is observed from the experimental results.

3) *Main Advantage of the proposed method*

In the proposed method in this paper, the uncertainty of the acceleration $\boldsymbol{R_{at}}$ is not constant and it is properly estimated to reflect the variation of active acceleration in different phases of motion. Thus, the inclination correction works well with fast convergence. In such a way, the balancing point from Fig. 14 is more precise. Modeling the acceleration uncertainty and take it into explicit account in the EKF formulation is critical to prevent large errors in inclination estimation and to improve the convergence of the result.

The proposed method is not aiming at tracking extremely dynamic motions for a long time, but it is focusing on the general sport motions with combination of fast and slow phases. In such a slow phase, the orientation can converge very efficiently. For example, Fig. 15 shows the tracking result for swinging motion with resting intervals. Tracking such general and periodic dynamic motions with bounded angular errors can be realized by this method.

B. *Analysis of Heading Error*

This paper does not provide a rigorous benchmark of the heading accuracy. But the applied tests indicate that the performance of the method in yaw correction is robust in a typical indoor environment. A more detailed study of the yaw estimation remains to be tested for different environment and longer durations. However, for now, it is confirmed that in a common indoor area, the proposed method can control the yaw error within a small range without significant effects from magnetic disturbances.

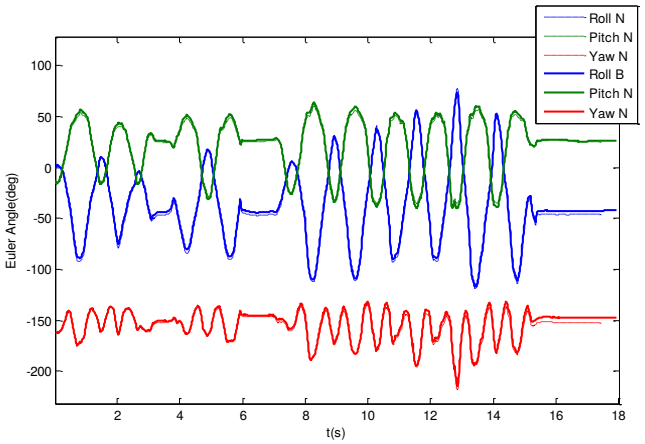

Fig. 15. Long Term Benchmark of Swinging Motion with Intermediate Stops (Roll N denotes the roll angel from the new algorithm, Roll B denotes the benchmark reference. Same for Pitch and Yaw)

VII. CONCLUSION

This paper proposed a robust and uncertainty based fusion method to track the 3D orientation of an object during dynamic motions through using low-cost IMU sensors. The active acceleration is mainly modeled as white noise, and the uncertainties of the active acceleration and the magnetic disturbances are accurately modeled accordingly. The sensor fusion algorithm is then formulated based on applying such uncertainties inside the EKF model. The proposed filtering approach is able to prevent large estimation errors due to the external and long-lasting accelerations, as well as due to the magnetic disturbances.

Such uncertainty estimation-based method makes the best use of the acceleration and the magnetometer measurements during the different phases of motion and corrects the orientation errors efficiently concerning the uncertainty values of unexpected disturbances in acceleration and magnetic field. The proposed method is also robust in the presence of acceleration shocks, and it converges quickly. Moreover, the method is also computationally efficient as it does not need to estimate the active acceleration.

The performance of this method has been benchmarked using the VICON OPTICAL capture system as the reference and compared with the estimations provided by XSENS MTw sensor. Results show that our method is more robust with less RMS errors in tracking motions. It is also more reliable in tracking actions with long-lasting high acceleration and the usage of the wearable IMU sensors could be extended to different types of motion tracking applications.

The more challenging and long-term dynamic situations are not studied in this work and the authors hope researchers to further research on tracking algorithms for long - term and extremely dynamic motions.

ACKNOWLEDGMENT

This work is supported in parts by the National Natural Science Foundation of China (51705076 and 51475448). The authors would like to thank Professor Qu Xingda in Shenzhen University on supporting with the equipment and thank

Assistant Professor Hu Xinyao and Mr. Jiang Jianxin for helping us with the experiments.

APPENDIX I. EXTENDED KALMAN FILTER (EKF)

The Extended Kalman filter (EKF) addresses the problem of estimating the state $\boldsymbol{x}$ of a discrete-time controlled process that is governed by non-linear stochastic difference equation,

$$\boldsymbol{x_k} = f(\boldsymbol{x_{k-1}}, \boldsymbol{u_{k-1}}, \boldsymbol{w_{k-1}}) , \quad (35)$$

with a measurement $\boldsymbol{z}$

$$\boldsymbol{z_k} = \boldsymbol{h}(\boldsymbol{x_k}, \boldsymbol{v_k}) . \quad (36)$$

The discrete-time controlled process to estimate the state is governed by the following difference equation

$$\boldsymbol{x_k^-} = f(\boldsymbol{x_{k-1}}, \boldsymbol{u_{k-1}}, \boldsymbol{0}), \quad (37)$$

The state error covariance matrix P_k can be initially projected as follows,

$$\boldsymbol{P_k^-} = \boldsymbol{A}\boldsymbol{P_{k-1}}\boldsymbol{A^T} + \boldsymbol{W_k}\boldsymbol{Q_{k-1}}\boldsymbol{W_k^T} , \quad (38)$$

where $\boldsymbol{A} = \frac{\partial}{\partial \boldsymbol{x}} f(\hat{\boldsymbol{x}}_{\boldsymbol{k-1}}, \boldsymbol{u_{k-1}}, \boldsymbol{0})$ $\boldsymbol{W_k} = \frac{\partial}{\partial \boldsymbol{w}} f(\hat{\boldsymbol{x}}_{\boldsymbol{k-1}}, \boldsymbol{u_{k-1}}, \boldsymbol{0})$, and $\boldsymbol{Q_{k-1}}$ is the process noise covariance matrix.

In EKF algorithm, the state correction is corrected based on the measurements as follows,

$$\boldsymbol{K_k} = \boldsymbol{P_k^-}\boldsymbol{H_k^T}(\boldsymbol{H_k}\boldsymbol{P_k^-}\boldsymbol{H_k^T} + \boldsymbol{V_k}\boldsymbol{R_k}\boldsymbol{V_k^T})^{-1} , \quad (39)$$

$$\boldsymbol{x_k} = \boldsymbol{x_k^-} + \boldsymbol{K_k}(\boldsymbol{z_k} - \boldsymbol{h}(\boldsymbol{x_k^-}, \boldsymbol{0})) , \quad (40)$$

where $\boldsymbol{H_k} = \frac{\partial}{\partial \boldsymbol{x}} h(\boldsymbol{x_k}, \boldsymbol{0})$ $\boldsymbol{V_k} = \frac{\partial}{\partial \boldsymbol{v}} h(\boldsymbol{x_k}, \boldsymbol{0})$, and $\boldsymbol{R_{k-1}}$ is the measurement noise covariance matrix.

The state error covariance matrix $\boldsymbol{P_k}$ is finally updated as follows,

$$\boldsymbol{P_k} = (\boldsymbol{I} - \boldsymbol{K_k}\boldsymbol{H_k})\,\boldsymbol{P_k^-} . \quad (41)$$

Initially $\boldsymbol{P_0}$ is given. If initial state has no error, it is set to be zero.

More detail information about EKF can be found in [28] .

REFERENCES

[1] E. Foxlin, "Inertial head-tracker sensor fusion by a complementary separate-bias Kalman filter," in *Virtual Reality Annual International Symposium, 1996., Proceedings of the IEEE 1996*, 1996, pp. 185-194, 267.

[2] E. Bachmann, "Inertial and magnetic tracking of limb segment orientation for inserting humans into synthetic environments.," PhD PhD Thesis, Naval Postgraduate School Monterey CA., Naval Postgraduate School, Monterey, California, 2000.

[3] M. Brodie, A. Walmsley, and W. Page, "Fusion motion capture: a prototype system using inertial measurement units and GPS for the biomechanical analysis of ski racing," *Sports Technology,* vol. 1, pp. 17-28, 2008.

[4] Y. Fujimori, Y. Ohmura, T. Harada, and Y. Kuniyoshi, "Wearable motion capture suit with full-body tactile sensors," in *IEEE International Conference on Robotics and Automation.*, Kobe, 2009, pp. 3186-3193.

[5] Y. Zhang, K. Chen, J. Yi, T. Liu, and Q. Pan, "Whole-Body Pose Estimation in Human Bicycle Riding Using a Small Set of Wearable Sensors," *IEEE/ASME Transactions on Mechatronics,* vol. 21, pp. 163-174, 2016.

[6] Qilong Yuan and I.-M. Chen, "Human Velocity and Dynamic Behavior Tracking Method for Inertial Capture System," *Sensors and Actuators A: Physical,* vol. 183, pp. 123-131, 2012.

[7] Qilong Yuan, I-Ming Chen, and S. P. Lee, "SLAC: 3D Localization of Human Based on Kinetic Human Movement Capture," in *IEEE International Conference on Robotics and Automation*, Shanghai, China, 2011, pp. 848 - 853.

[8] D. Vlasic, R. Adelsberger, G. Vannucci, J. Barnwell, M. Gross, W. Matusik, *et al.*, "Practical motion capture in everyday surroundings," *ACM Transactions on Graphics (TOG),* vol. 26, pp. 35-44, 2007.

[9] C. N. Teague, S. Hersek, H. Töreyin, M. L. Millard-Stafford, M. L. Jones, G. F. Kogler, *et al.*, "Novel Methods for Sensing Acoustical Emissions From the Knee for Wearable Joint Health Assessment," *IEEE Transactions on Biomedical Engineering,* vol. 63, pp. 1581-1590, 2016.

[10] P. C. Lin, J. C. Lu, C. H. Tsai, and C. W. Ho, "Design and Implementation of a Nine-Axis Inertial Measurement Unit," *IEEE/ASME Transactions on Mechatronics,* vol. 17, pp. 657-668, 2012.

[11] K. Parsa, T. A. Lasky, and B. Ravani, "Design and Implementation of a Mechatronic, All-Accelerometer Inertial Measurement Unit," *IEEE/ASME Transactions on Mechatronics,* vol. 12, pp. 640-650, 2007.

[12] G. Chelius, C. Braillon, M. Pasquier, N. Horvais, R. P. Gibollet, B. Espiau, *et al.*, "A Wearable Sensor Network for Gait Analysis: A Six-Day Experiment of Running Through the Desert," *IEEE/ASME Transactions on Mechatronics,* vol. 16, pp. 878-883, 2011.

[13] "MTw User Manual, MTw Hardware, MT Manager, Awinda Protocol ", https://www.xsens.com/, 2018.

[14] M. A. D. Brodie, "Development of fusion motion capture for optimization of performance in alpine ski racing," PhD Thesis, Massey University, Massey University, 2009.

[15] H. Luinge, "Inertial sensing of human movement," PhD Thesis, Universiteit Twente, 2002.

[16] D. Roetenberg, "Inertial and magnetic sensing of human motion," PhD Thesis, Universiteit Twente, 2006.

[17] A. M. Sabatini, "Kalman-Filter-Based Orientation Determination Using Inertial/Magnetic Sensors: Observability Analysis and Performance Evaluation," *Sensors,* vol. 11, pp. 9182-206, 2011.

[18] M. A. Brodie, A. Walmsley, and W. Page, "Dynamic accuracy of inertial measurement units during simple pendulum motion," *Computer Methods in Biomechanics & Biomedical Engineering,* vol. 11, pp. 235-42, 2008.

[19] L. Ricci, F. Taffoni, and D. Formica, "On the Orientation Error of IMU: Investigating Static and Dynamic Accuracy Targeting Human Motion," *Plos One,* vol. 11, p. e0161940, 2016.

[20] T. Pfau, T. H. Witte, and A. M. Wilson, "A method for deriving displacement data during cyclical movement using an inertial sensor," *Journal of Experimental Biology,* vol. 208, pp. 2503-14, 2005.

[21] S. A. Skogstad, K. Nymoen, Y. de Quay, and A. Jensenius, "OSC Implementation and Evaluation of the Xsens MVN suit," in *Proceedings of New Interfaces for Music Expression, Oslo, Norway*, 2011, pp. 12-35.

[22] J. K. Lee, E. J. Park, and S. N. Robinovitch, "Estimation of attitude and external acceleration using inertial sensor measurement during various dynamic conditions," *IEEE transactions on instrumentation and measurement,* vol. 61, pp. 2262-2273, 2012.

[23] I. Skog, P. Handel, J. O. Nilsson, and J. Rantakokko, "Zero-Velocity Detection—An Algorithm Evaluation," *IEEE transactions on bio-medical engineering,* vol. 57, pp. 2657-2666, 2010.

[24] E. Foxlin, "Pedestrian Tracking with Shoe-Mounted Inertial Sensors," *IEEE Computer Graphics & Applications,* vol. 25, pp. 38-46, 2005.

[25] E. R. Bachmann, R. B. McGhee, X. Yun, M. J. Zyda, and D. L. McKinney, "Method and apparatus for motion tracking of an articulated rigid body," ed: Google Patents, 2004.

[26] X. Yun, C. Aparicio, E. R. Bachmann, and R. B. Mcghee, "Implementation and Experimental Results of a Quaternion-Based Kalman Filter for Human Body Motion Tracking," in *IEEE International Conference on Robotics and Automation*, 2005, pp. 317-322.

[27] R. Murray, Z. Li, S. Sastry, and S. Sastry, *A mathematical introduction to robotic manipulation*: Boca Raton,FL, 1994.

[28] G. Welch and G. Bishop, "An introduction to the Kalman filter," pp. 1-16, 1995.

[29] G. Bellusci, F. Dijkstra, and P. Slycke, "Xsens MTw: Miniature wireless inertial motion tracker for highly accurate 3D kinematic applications," *Xsens Technologies,* 2013.

[30] E. Bachmann, "Inertial and magnetic tracking of limb segment orientation for inserting humans into synthetic environments.," PhD Thesis, Naval Postgraduate School Monterey CA., 2000.